Journal Pre-proofs

Ocher deposit prospecting using object-based image analysis of WorldView-3 VNIR data: A case study in Hormuz Island, southern Iran

Samira Shayeganpour, Majid H. Tangestani, Saeid Homayouni, Pece V. Gorsevski

Please cite this article as: Shayeganpour, S., Tangestani, M.H., Homayouni, S., Gorsevski, P.V., Ocher deposit prospecting using object-based image analysis of WorldView-3 VNIR data: A case study in Hormuz Island, southern Iran, *Advances in Space Research* (2023), doi: https://doi.org/10.1016/j.asr.2023.03.049

This is a PDF file of an article that has undergone enhancements after acceptance, such as the addition of a cover page and metadata, and formatting for readability, but it is not yet the definitive version of record. This version will undergo additional copyediting, typesetting and review before it is published in its final form, but we are providing this version to give early visibility of the article. Please note that, during the production process, errors may be discovered which could affect the content, and all legal disclaimers that apply to the journal pertain.

Ocher deposit prospecting using object-based image analysis of WorldView-3 VNIR data: A case study in Hormuz Island, southern Iran

Samira Shayeganpour[1], Majid H. Tangestani[*1], Saeid Homayouni[2], Pece V. Gorsevski[3]

[1]Department of Earth Sciences, Faculty of Sciences, Shiraz University, Shiraz, Iran

[2]Insitut National de la Recherche Scientifique, Centre Eau Terre Environnement, Québec, Canada

[3] School of Earth, Environment and Society, Bowling Green State University, Bowling Green, Ohio, United States

* Corresponding author; Majid H. Tangestani; Email:tangstan@shirazu.ac.ir

Abstract

Mapping lithological units and conducting mineral exploration in a relatively short time and at a reduced cost, requires high-resolution satellite data and state-of-the-art image processing approaches and methods. In this regard, the current paper aims to test an integration of visible-near infrared imagery from WorldView-3 (WV-3) and object-based classification for mapping potential deposits of ocher in Hormuz Island, southern Iran. A combination of field observations, spectroscopy, microscopic mineralogy, and geochemical-based XRD and XRF analyses were conducted on the samples collected throughout the study area. The reflectance and absorption features of the ocher were extracted from spectroscopic measurements of samples from well-known ocher mines at the area, and were then convolved to the WV-3 bands. Results showed that the spectral characteristics of ocher are governed by iron oxides and clay minerals with a presence of distinct strong absorption and high reflectance features in the 510-625 nm and 630-745 nm wavelength regions, respectively. These features are complemented by molecular vibration processes of water O-H intramolecular stretching and H–O–H bending that generate absorption features in the 1440-1940 nm region. Additional absorption features in the 2210-2300 nm are most likely due to the Al-OH and CO_3^{-2} vibrations. The absorptions centered at 480 nm, 540 nm, and 820 nm correspond to bands 2, 3, and 7 of the WV-3, respectively, whereas the high reflectance feature centered near 700 nm corresponds to band 6. These four bands, which were considered as index bands of ocher in this study, were used to assign the segmentation weights and to create the thresholds during image processing. Brightness, density, compactness, and homogeneity features were the primary factors for selecting the training areas in the index bands. The ocher-rich areas were enhanced by using a two-stepapproach of object-based image analysis (OBIA) and image classification, for suitable threshold selection. The information about the feature variables of the ocher within the image and lithological object hierarchy were obtained to evaluate the features of ocher deposits. Information extracted from the index bands provided an important description of the object features, including mean, standard deviation, minimum and maximum pixel values, hue, saturation, and intensity, while the training areas obtained information from the three known ocher mines. Considering the fixed numerical range of ocher mines as a reference, the fixed numerical range of general and specific features of ocher in index bands of WV-3 were achieved. The numerical ranges of pixels were used for creating threshold conditions when applying the "assign class" algorithm in bands 2, 3, and 7 are 815-975 nm, 930-1052 nm, and 1721-

1904 nm, respectively. The presented OBIA approach shows a high potential with an overall accuracy of 88 % to discriminate deposits of ocher based on compatibility between ocher mines and identified ocher-bearing pixels.

Keywords: remote sensing, WV-3, OBIA, Hormuz Island, ocher

1. Introduction

Salt domes are geological structures formed through deformation events and/or diapirism, where lighter materials such as salt rise to the surface. The occurrence of salt domes with specific lithology and evolving history creates a specific morphology and potential for prospecting metal and non-metal deposits such as halite, potash, ocher, gypsum, oligist, and dolomite (Ghorbani, 2013). Specifically, the Hormuz Formation, which is exposed in over 200 salt domes in the Zagros Mountains, dominantly consists of a mixture of igneous and sedimentary rocks, and is susceptible for mineral exploration. The Hormuz Island, which is located in the Strait of Hormuz, southern Iran, is a salt dome that consists of salt rock (halite), gypsum, carbonate, intrusive and volcanic rocks, low-grade metamorphic, and detrital sedimentary rocks (Faramarzi et al., 2015). The salt domes, particularly the Hormuz Island, are not only important for considerable mineral resources but also for geo-tourism (Faramarzi et al., 2015; Yazdi et al., 2014). The ocher or the red soil deposits on the Hormuz Island are iron-rich and colored with hydrated iron oxides that are used as a natural pigment. Although the red ocher is dominant, various shades of yellow, purple, sienna, and umber are also observed in the landscapes. Moreover, ocher is a non-toxic material that can be used in chemical, pharmaceutical, cosmetic, and textile industries; however, it is mostly used in the paints and artwork industries (Dwevedi et al., 2017). The Hormuz ocher mine, which is located in the southern area of this island is well known for the red-colored earth pigment, and more than 390,000 tons of ocher with 30% hematite is annually extracted from it (Yazdi et al., 2014).

Mapping, monitoring, and evaluating mineral deposits at large scales in a timely and efficient manner and at a reduced cost, requires new tools such as high-resolution satellite data and advanced digital image processing approaches and methods. However, many lithological and mineral mapping projects have recently relied on the applications of optical remote sensing imagery such as multispectral data from Landsat and the Advanced Space borne Thermal Emission and Reflection Radiometer (ASTER) sensor, onboard the Terra satellites. Many surface materials have already been enhanced and reported through integrated approaches of different field data collection and image processing techniques applied to spectral bands in the visible (VIS), near-infrared (NIR), and shortwave infrared (SWIR) regions of the electromagnetic spectrum (Karale et al., 1983; Singh, 2016; Escribano, 2017). However, unlike the Landsat TM and ASTER, the WorldView-3 (WV-3) imagery offers higher spatial, spectral, and radiometric resolutions, which create opportunities for detailed mapping and monitoring of lithology, hydrothermal alteration of minerals, land use/ land cover (LULC), soil, and other environmental applications. WV-3 is a high-resolution commercial satellite operated by Maxar company that provides eight multispectral bands in the visible and near-infrared (VNIR) region, and eight bands in the SWIR region. By taking advantage of absorption and reflection features of the desired targets, both simulated and raw imagery of WV-3 have recently been used in geological studies for mineral enhancement and lithological mapping (Hewson et al., 2019; Karimzadeh & Tangestani, 2021; Kruse & Perry, 2013; Mars, 2018; Ye et al., 2017). However, additional research is necessary to increase understanding of absorption and reflection features of materials such as ocher in WV-3 bands, since no publication or research work is available to date.

Some of recent works on lithological mapping have extended pixel-based image analysis by coupling object-based image analysis with WV-3 (e. g., Karimzadeh & Tangestani, 2021). OBIA is a digital image analysis technique based on objects, composed of groups of pixels with similar spectral properties (Burnett & Blaschke, 2003; Blaschke et al., 2004). For instance, in this research the image segmentation algorithm splits an image into ocher and non-ocher object elements based on the introduced properties such as shape, size, color, and linked topology. In addition, the segmented image objects can be categorized by unsupervised, supervised, soft (i.e., fuzzy) or rule-based classification approaches using property similarities (Lang et al., 2008). The usefulness of OBIA includes the possibility of incorporating user-controlled inputs for meeting a specific objective (i.e., controlling object-level shape or texture), the possibility for smoothing local variations, and implementation of a nested hierarchy of objects (i.e., multiple levels of object subsets). Nevertheless, integrating semantic and expert-based knowledge in OBIA requires a meaningful and representative object homogeneity (Blaschke et al., 2004).

The implementation of OBIA in geosciences has mostly been focused on land cover and mineral mapping based on the classification of high-resolution remote sensing imagery (Thomas et al., 2011; Grebby et al., 2016; Serbouti et al., 2021; Shayeganpour et al., 2021a, 2021b). Some of the OBIA-based research suggests that exploration of iron deposits and gossan minerals has substantially been improved by the use of Landsat and ASTER data (Pour and Hashim, 2012; Yang, 2015; Eslami et al., 2015). However, very few applications, especially in mineral exploration, have tested the capabilities of OBIA with high-resolution imagery. Thus, the implementation of OBIA with high-resolution imagery could be a new challenge in both image analysis and mineral exploration since very few remote sensing publications have proposed iron oxide/hydroxide mapping from WV-3 (Bedini, 2019; Salehi and Tangestani, 2019; Sun et al. 2017).

To date, many methods and algorithms with different strengths and efficiencies have been applied for classifying the satellite images (e. g., Congalton, 1991; Shayeganpour et al. 2021a), exploration of minerals (e. g., Bedini, 2019; Salehi and Tangestani, 2019), and discrimination of rock types (e. g., Forouzan and Arfania, 2020). Identifying target minerals based on spectral features and index bands is a method with relatively high efficiency which could be further improved by incorporating high spatial and spectral resolution data such as from WV-3.

The principal aim of this research is to improve the applicability of existing image processing methods through integration of field observations, OBIA, and WV-3 data. For this purpose, the index bands of ocher in WV-3 dataset were obtained from spectral properties of its well-known mines in the study area to be used as basis for a threshold classification method. Specifically, the steps of this research included: 1) collection of ocher spectra, recognition of spectral features from available spectral libraries, and extraction of representative ocher index bands from the VNIR dataset of WV-3; 2) enhancement of ocher enriched areas by the use of OBIA and threshold classification algorithms; and 3) assessment of capability of OBIA and WV-3 for exploration of ocher in a lithologically complex terrain.

2. Geology

Hormuz Island is the most famous salt dome at the Persian Gulf (Fig. 1-a) and consists of a variety of sedimentary and igneous rocks of Late Precambrian to Tertiary. This island which has emerged from water about 50,000 years ago (Yazdi, 2013) is dominantly composed of evaporate rocks, ferruginous formations, and sediments (Elyasi et al., 1975). Besides evaporates, detrital sedimentary and igneous rocks can be found in the so-called Hormuz Formation or series,

outcropped in this island. Stocklin (1972) concluded that the Hormuz series consists of red soil, salt layers, gypsum, sandy rocks, dolomite, and limestone, which are expanded between Oman-Naiband lineament in the east and the Qatar-Kazeroun lineament, southwestern Iran. The research also reported various magma activities in the forms of extrusive and intrusive bodies in two phases; the first included basalt and diabase, and the second consisted of rhyolite, rhyodacite, and trachyte. The igneous rocks produced by the volcanic activities, except rhyolite, which is somehow intact, are dominantly altered.

The rock units of study area were nominated based on the previous studies (Elyasi et al., 1975; Shayeganpour et al., 2021) and field observations in 125 sampling stations (Figs. 1-b and 2). The lithological units were classified as mixtures of red soil, tuff and anhydrite; red soil, gypsum, and anhydrite, diabase and volcanic tuff, as well as unmixed units of white rhyolite tuffs, and marl (Figs. 1b and 2). The center of the island is a dome cap that is composed of salt, anhydrite, dolomite, basic igneous rocks, and red siltstone, while its rim is composed of evaporates alternating with dark dolomite, rhyolite, tuffaceous and micaceous sandstone and mudstone, and rarely of conglomerate beds (Aqanabati, 2006; Nabavi & Agha Nabati). Figure 1-b shows the ocher mines outlined by yellow boxes. The material form the mines is extracted and transferred into a processing plant (Fig. 3) that is located in the northeastern part of the island (Bosak et al., 1999).

Ocher is a natural clay earth pigment, a mixture of ferric oxide and varying amounts of clay, silt, and sand, which ranges in color from yellow to deep orange or brown. The processes of iron oxide formation in ocher include the release of Fe^{3+} ions which migrate to the deep settings where intermediate compound of $Fe(OH)_3$ is formed and transformed into Fe_2O_3. The main properties that determine the ocher quality and its industrial consumption include enveloping power, luster, particle size, and mineralogical composition.
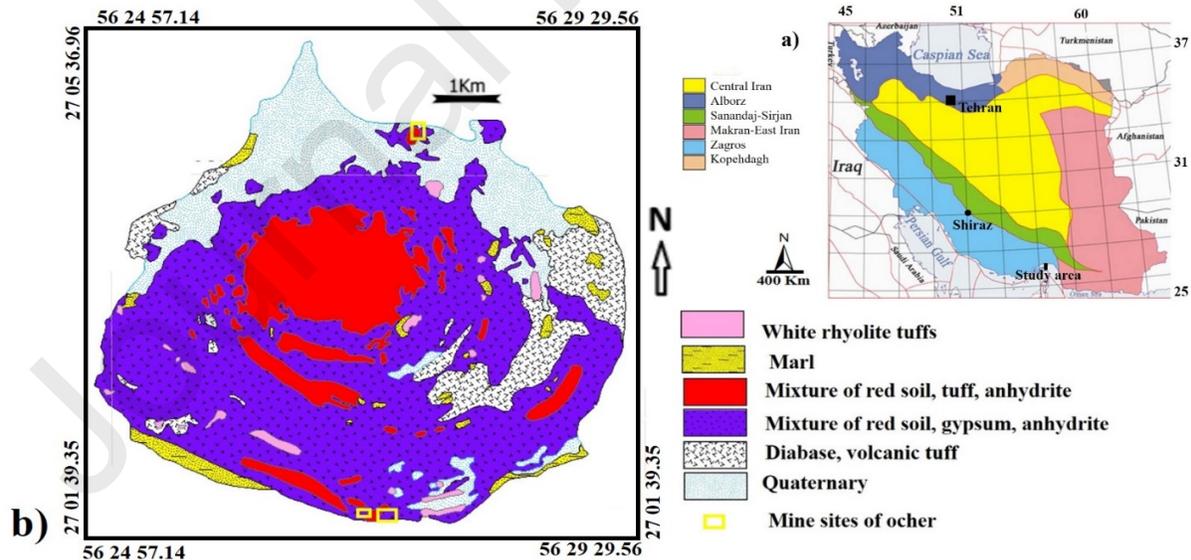

Fig. 1. (a) location of the study area in map of Iran (red circle), (b) simplified geological map of Hormuz Island based on Elyasi et al. (1975) and Shayeganpour et al. (2021).
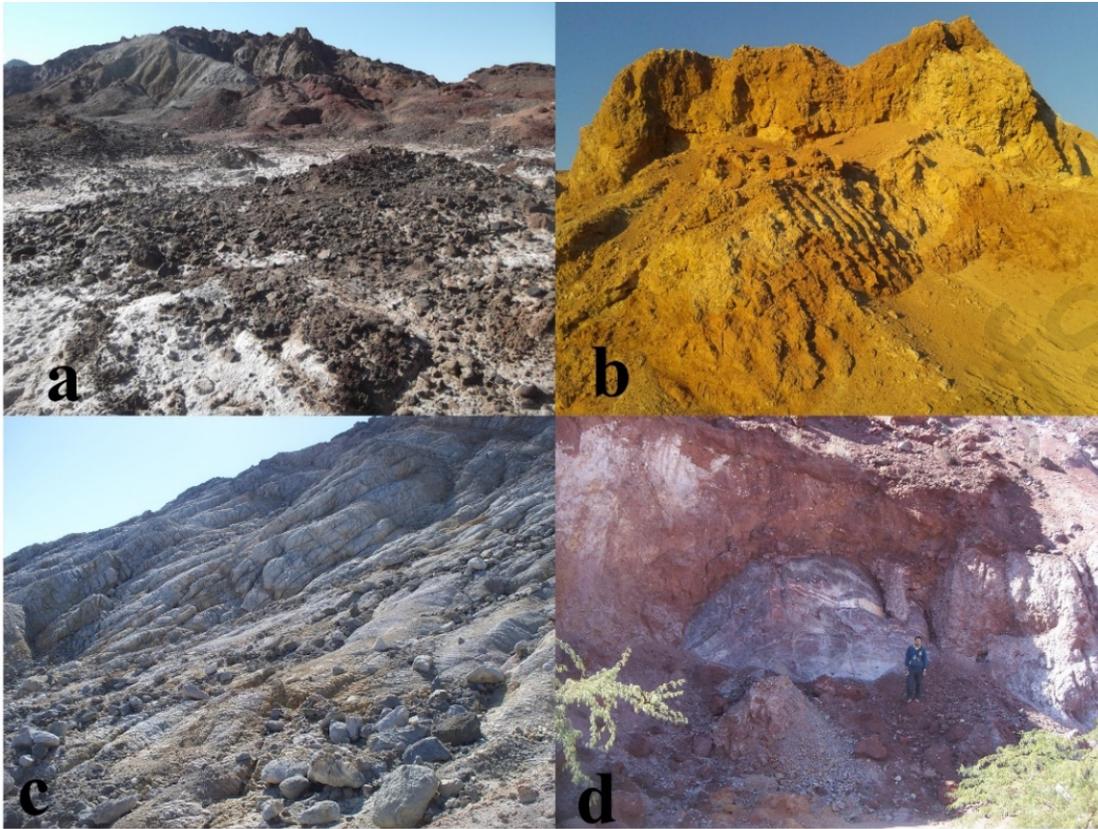
Fig. 2. Field view of the lithological units in Hormuz Island: (a) diabase and volcanic tuff, (b) marl; c) white rhyolite tuffs, and d) mixture of red soil, gypsum and anhydrite.
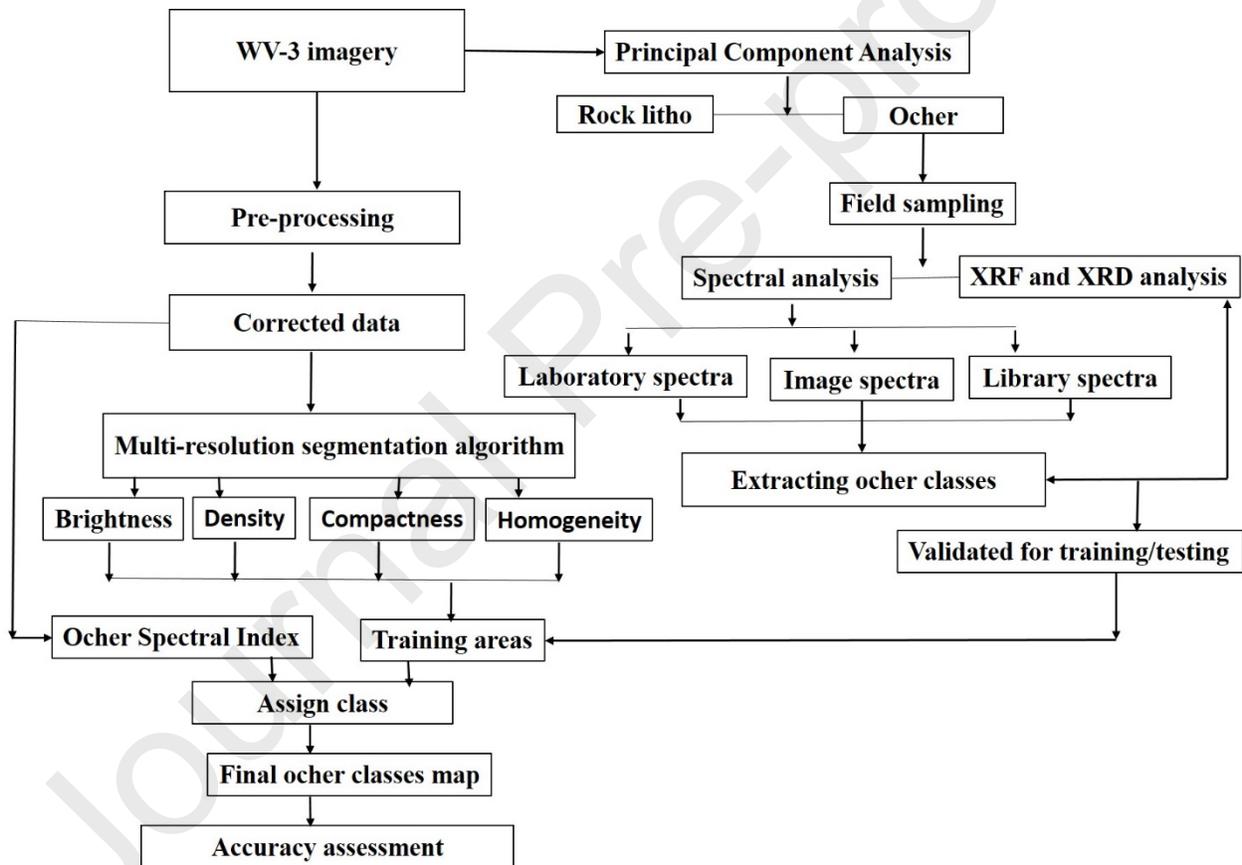

Fig. 3. The ocher mine (a) and ocher processing plant (b) in Hormuz Island.

3. Materials and Methods

The usefulness of the VNIR data from WV-3 for potential mapping of ocher deposits was assessed through integration of field observations and sampling, mineralogical and lithological investigations of microscopic thin sections,

measurement and analysis of spectral features, image processing, and geochemical analyses using X-ray diffraction (XRD) and X-ray fluorescence (XRF) methods. The flowchart of the methodology for processing the data is summarized in Figure 4. Based on the field observations and available reports from the Geological Survey of Iran, the locations of active ocher mines were identified, and 125 samples were collected throughout the study area. Among the samples, a total of 80 samples were investigated to identify the lithological units and a total of 45 samples were used for verifying the ocher anomalies. The spectral properties of ocher samples in VNIR-SWIR regions were measured by a spectrometer and the results were investigated in both a high-resolution mode and for the spectra convolved to WV-3 bands. The applied VNIR imagery were firstly corrected for possible geometric and atmospheric errors, and were then processed by the use of OBIA and classification approaches. A confusion matrix was finally calculated to assess the accuracy of the results.

Figure 4. Flowchart diagram showing the methodology of data processing framework

3.1. Spectral Features

Spectral features of samples were measured in the range of 0.4 μm to 2.5 μm using an ASD FieldSpec spectrometer at the Department of Geology, Bowling Green State University, USA, and a NIRS (Near-infrared spectroscopy) instrument, active in the Central Laboratory of Shiraz University, Shiraz, Iran. The measurements were performed on both the field-collected rock samples and the ocher samples collected from known mines in a single reading mode. Based on the exploration purposes, the ocher spectral properties were analyzed and presented in this paper. These

features were investigated by means of high-resolution reflectance spectroscopy, and based on the spectra of samples resampled to the WV-3 spectral bands. Finally, the correspondence of measured spectral features with mineralogy and lithology of collected samples and the field observations was analyzed.

3.2. Remote Sensing Data

WV-3 is a commercial satellite which consists of 16 spectral bands in the VNIR and SWIR regions of the electromagnetic spectrum. It was launched by the Digital Globe on August 13th, 2014. This satellite operates at an altitude of 617 kilometers and provides a panchromatic band with pixel size of 31-centimeter, 8 VNIR bands with pixel size of 1.24-meter, and eight bands in the SWIR region with 3.7-meter pixel size (Kuester, 2016). These data are available for conventional applications in the range of 400 to 1040 nm for the eight visible and near-infrared bands, and in 1195 to 2365 nm for the eight SWIR bands. The spatial resolution of NIR and SWIR bands has been degraded to 7.5 m for public use based on licensing privileges. The data utilized in this study were in level 2A, which included one panchromatic and 8 VNIR bands (Table 2), acquired at 2:00 pm on June 16th, 2016. The level 2A are standard data, partly corrected for radiometric errors and geo-registered based on UTM projection system and datum of WGS84.

Table.2. Characteristics of the VNIR bands of WV-3

Spectral range	Band name	Spectral band	GSD (Ground Sample Distance)
Panchromatic Band (1)		450 - 800 nm	Nadir: 0.31 m, 20º off-nadir: 0.34 m
MS (Multispectral) Bands (8) in VNIR (Visible Near Infrared)	Coastal Blue	400 - 450 nm	Nadir: 1.24 m 20º off-nadir: 1.38 m
	Blue	450 - 510 nm	
	Green	510 - 580 nm	
	Yellow	585 - 625 nm	
	Red	630 - 690 nm	
	Red edge	705 - 745 nm	
	Near-IR1	770 - 895 nm	
	Near-IR2	860 - 1040 nm	

3.3. Pre-processing

WV-3 imagery used in this study were previously geo-referenced to UTM projection zone 40 North and WGS84 datum. Following the initial step of preparation, the pre-processing included radiometric calibration, atmospheric correction, and removal of the interference factors. The radiometric calibration used Equation (1) to convert the 16-bit digital numbers of pixels into the physical radiance at the top of the atmosphere (Zhang et al., 2008; Chen et al., 2014; Sun et al., 2017).

$$L = \frac{DN * AbsCalFactor}{\Delta\lambda}$$ Equation (1)

7

In this equation; L (W m^{-2} sr^{-1} mm^{-1}) is the radiance, Δλ (μm) is the effective bandwidth, and "AbsCalFactor" is the absolute calculation factor. The parameters such as "AbsCalFactor" and "Δλ" reside in a metadata file with an extension "IMD", which is distributed with the original datasets.

Atmospheric correction removes the scattering and absorption effects from the atmosphere, where top-of-atmosphere radiance is converted into surface reflectance. For this purpose, we applied the Fast Line-of-sight Atmospheric Analysis of Spectral Hypercubes (FLAASH) correction algorithm, available in the ENVI (Environment for Visualizing Images) software, version 5.3. This algorithm that uses the MODTRAN radiative transfer model code, has extensively been used for the hyperspectral and multispectral data processing. It is capable of extracting the parameters converted to surface reflectance (Luo et al., 2009).

Considering that the study area is an island, sea water was the principal interference factor. In this regard, a masking approach was used to separate the land from its water background at all the bands (Fig. 5). Moreover, a threshold range of 0.00 < VNIR-1 < 4.62 was used to avoid losing the dark pixels.

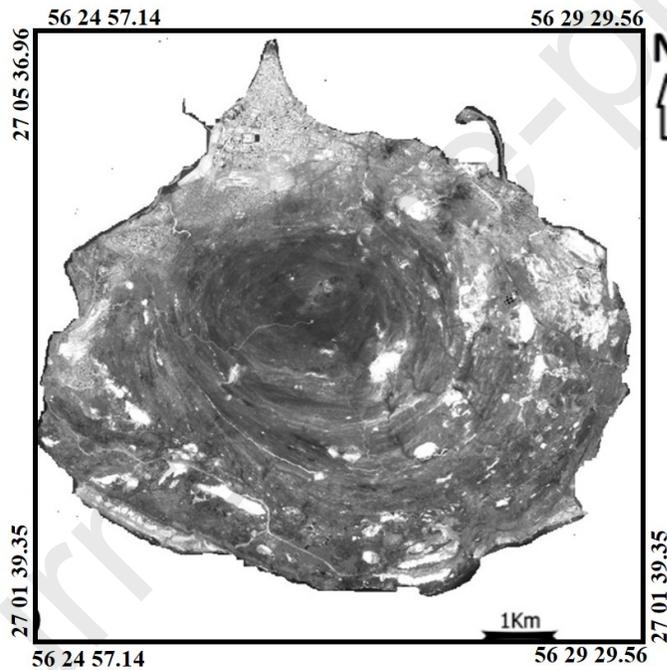**Fig. 5.** Map of study area depicting Hormuz Island after masking the surrounding sea water (band 2 from WV-3)

3.4. Object-Based Image Classification

The image processing steps for mapping of ocher-rich areas in the Hormuz Island included identification of index bands (i.e., bands with characteristic absorption and reflection features), segmentation of WV-3 data, and algorithm execution for enhancing the desired class through a thresholding approach.

In order to define the weights of the index bands based on the spectral characteristics, the data points were projected in *n*-space onto the axes with proper model units for scaled radiance or reflectance and vector directions. Similar to

the principal component analysis (PCA) technique, this orthogonal transformation process of the original data reduces the band space and depicts specific spectral patterns associated with the index bands (Kauth & Thomas, 1976).

The OBIA approach and a classification algorithm were used to detect the potential ocher deposits from the atmospherically corrected WV-3 bands. The first step in OBIA was partitioning the image by segmentation approach which is a technique that groups individual pixel value of the image to a particular class. When performing this approach, the image objects are created or the morphology of the current image objects are altered based on the particular criteria (Blaschke and Burnett, 2004). The assignment of classes (objects), subclasses, and un-classes is based on a supervised classification approach using the "assign class" tool; among which, the known ocher mines were assigned to "class parameter", accordingly. The membership value for the ocher class was set to 1 for all objects, and the non-ocher class was set to 0. As part of the domain, the threshold condition for process-based classification was also set to the applied algorithm. The defined threshold creates a limit in classifying objects in the image and restricts the algorithm's performance to only those within the limit range. In the thresholding step, it is possible to assign image objects to a class based on only one condition or combining several conditions using various thresholds based on different features.

3.5. Accuracy Assessment

In order to assess the accuracy of the results, a confusion matrix (Congalton 1991) was calculated, and the producer's and user's accuracies were determined. While the producer's accuracy (omission error) depicts the correctness of a real feature on the classification map, the user's accuracy (commission error) depicts whether the classified feature represents that category on the ground. An integration of field observations, XRD and XRF analyses, and reflectance spectroscopy were used to verify the agreement of the potential areas identified as ocher deposits. The ground truthing dataset for the accuracy assessment was established from data collected at the known ocher mines.

4. Results and Discussion

4.1. Spectral features of ocher

The high-resolution spectra of ocher samples (Fig. 5) showed absorption features in the 450-540 nm region, as well as at specific wavelength locations centered at 860 nm, 1440 nm, 1940 nm, 2210 nm, and 2330 nm. The absorption, in the 450-540 nm region and the 860 nm wavelength location, which are shown in all spectra, could be attributed to iron oxide (hematite, Fe_2O_3). The high reflectance near 700 nm caused red color in field samples. A comparison of the measured spectra of ocher samples with similar spectra available in the USGS spectral library (https://www.usgs.gov), showed that the ocher spectral features are compatible with the spectra of hematite (Fe_2O_3), goethite (FeO-OH), and limonite ((FeO (OH) nH_2O)) (Clark et al., 2007; Hunt, 1977) showing a sharp fall-off in the blue region (400-570 nm) due to the charge-transfer effect in Fe-O, as well as high reflectance in 740 nm and > 870 nm. The occurrence of Fe^{3+} and Fe^{2+} in hematite, limonite, and goethite, as the significant ocher phases, are the major reasons for absorption features in this material. The diagnostic absorption features of Fe^{2+} are near 510 nm, 550 nm, and 1200 nm, while these features are near 490 nm and 870 nm for Fe^{3+}. Moreover, the first OH-stretching overtones, the combinations of the H–O–H bending with the OH stretching, asymmetric O–H stretching, and H–O–H bending

are the major factors for absorption features near 1440 nm and 1940 nm in iron hydroxides (Gaffney et al. 1984; Clark et al. 1990; Bishop et al. 1994). Other water-bearing minerals including clay group such as illite and muscovite, and evaporate minerals such as gypsum and anhydrite can also show these absorption features (Cloutis et al. 2002). The absorption feature at 2210 nm (Fig. 6) is for the presence of Al-OH in clay minerals, which occur as major phases in ocher. Thus, the minor absorption feature near 2300 nm identified in a few ocher samples could be linked to CO_3^{2-} in carbonate minerals (Clark et al. 1990).

When resampling the spectra of field samples to WV-3 VNIR bands, the absorption features in 480 nm, 540 nm, and 820 nm were, respectively, compatible with bands 2, 3, and 7, whereas the high reflectance in 700 nm was matched to band 6.
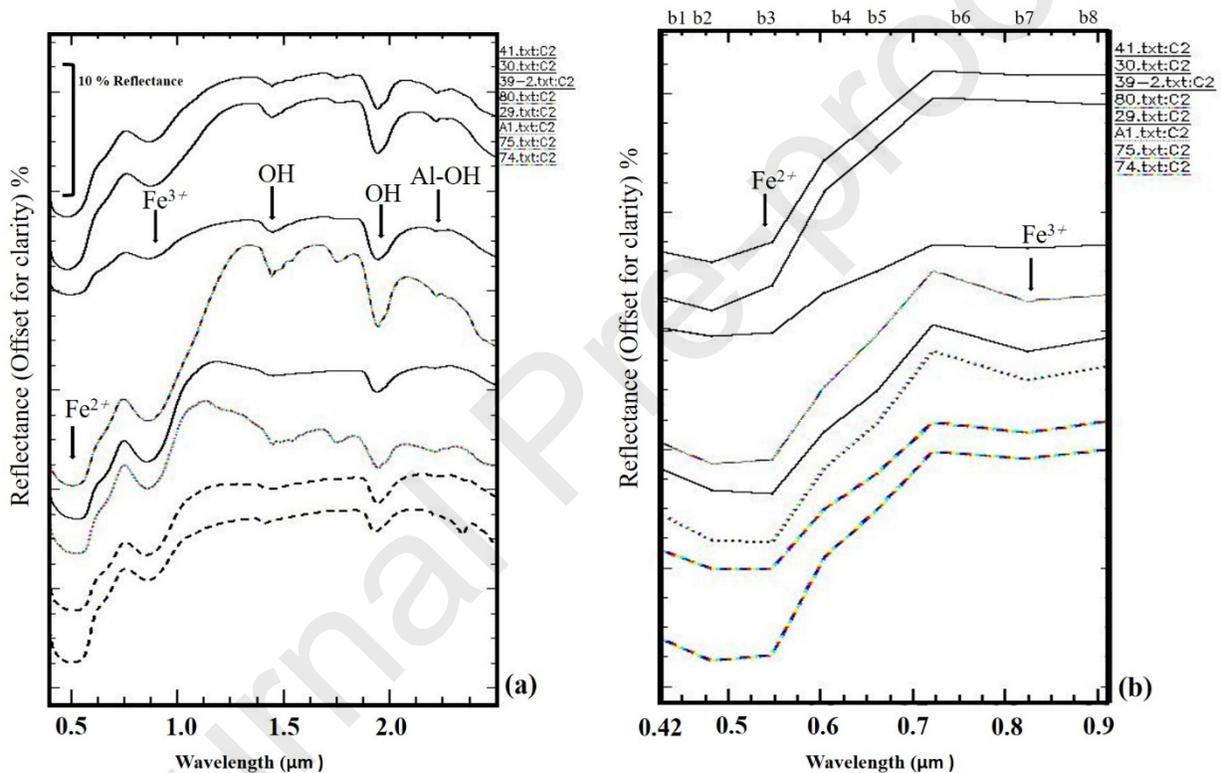

Fig. 6. Reflectance spectral curves of ocher; a) high-resolution spectra of field samples, and b) spectra resampled to the WV-3 bands (details of spectra are described in the manuscript; the legend of each figure shows the sampling number).

4.2. Ocher Spectral Index

The OBIA approach uses the index bands to analyze the object-based classes by the use of spectral indicators. These indicators are, in fact, provided on the basis of the previously selected bands called sensitive (or index) bands. In order to map the ocher-rich potentials in the study area, the blue, green, yellow, red, NIR-1, and NIR–2 bands of the WV-3were selected to aid the intended data processing. Salehi and Tangestani (2019) suggested that using these spectral bands can successfully identify the iron oxides/hydroxides. The lack of the vegetation cover coupled with arid climate

10

in the Hormuz Island have led to the exposure of rock units and the surface iron oxides/hydroxides to the satellite view. Based on the high-resolution spectral analysis (section 4.1) of measured samples, the diagnostic absorption features of ocher are similar to the spectra of a mixture of iron oxide/hydroxide and clay minerals.

The spectral features of target minerals in the USGS spectral library, resampled to the applied WV-3 spectral bands, are shown in Figure 7 (a). As revealed in this figure, the diagnostic absorption features of hematite are near 480 nm, 540 nm, and 820 nm, while for limonite and goethite, they are near 480 nm and 910 nm. Moreover, Figure 7 (b) shows that bands 2, 3, 7, and 8 coincide with the strong absorption features near 480 and 550 nm as well as the broad and shallow absorption features near 820 nm and 910 nm, respectively. Based on the fact that the spectral characteristics of ocher are more similar to the spectral features of iron oxide and hydroxides, which show strong absorption in the 510-625 nm region and high reflection in the 630-745 nm region, bands 3 and 4 were chosen as absorption indicators, and bands 5 and 6 as indices for high reflection. This interpretation of spectral features and extraction of index bands helped with the choice of weights for segmentation, feature selection, and creation of threshold conditions in the subsequent image processing.
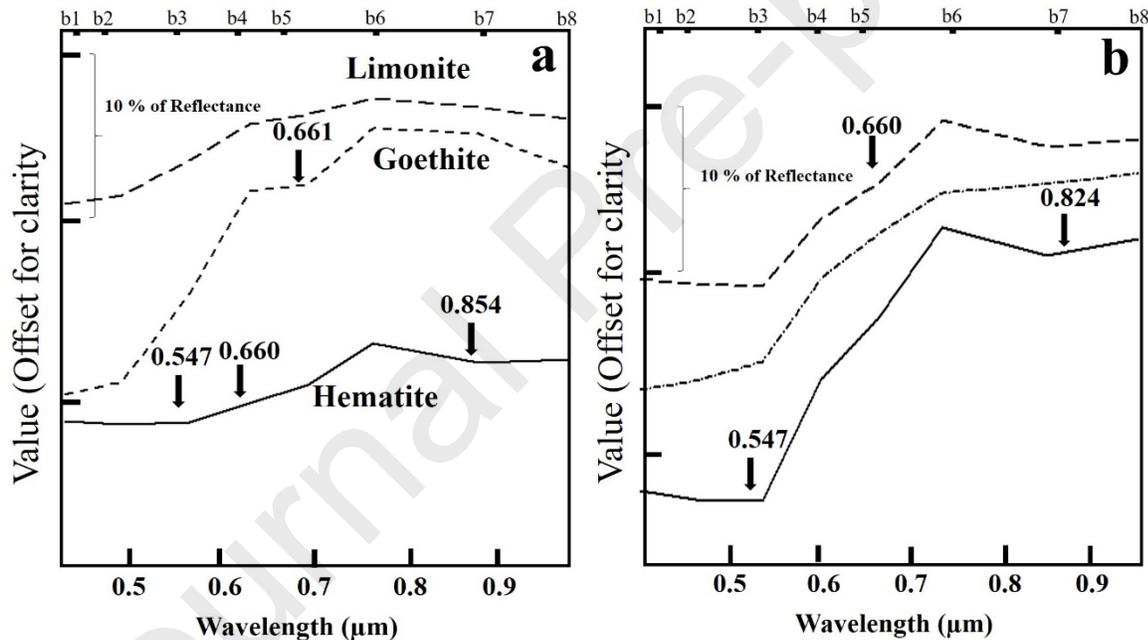

Fig. 7. a) Reflectance spectra of hematite, limonite, and goethite of the USGS spectral library, resampled to the WV-3 VNIR bands; b) reflectance spectra of ocher samples resampled to the same bands (spectral characteristics of samples are explained in the main body of the manuscript).

4.3. Segmentation

Before performing a classification method based on the threshold approach, the WV-3 images were segmented based on the index bands. Tormos et al. (2012) suggested two approaches for segmentation: 1) subdividing a big feature into smaller fragments, which is a top-down strategy; and 2) combining the small fragments into larger feature, which is a bottom-up approach. In this paper, we applied the bottom-up strategy to enhance the potentials of ocher deposits.

11

When using this strategy, the multi-resolution segmentation of the image initiates at the pixels' level. The advantages of bottom-up segmentation include high simplicity, the fact that it can extend any single change point detection method to discern multiple change points, and that it can work whether the number of patterns is already known or not. Using the relative homogeneity criteria, the multi-resolution segmentation algorithm composes an image object from individual cells by iterative merging of neighboring cells. A combination of the spectral and shape properties was used to define the homogeneity criteria. The first and the major parameter in the segmentation setting is to weigh the selected bands in the image layer. Considering the spectral features of iron oxides, weight 4 was assigned to the high absorption bands 2 and 7, and weight 2 was assigned to the high reflections bands 5 and 6 and the moderate absorptions bands 3 and 4. Assigning higher weights to the absorption bands plays a critical role in the enhancement of desired targets.

The parameters associated with the "composition of homogeneity criterion in the shape section" and "value of compactness" were set to 0.9 and 0.5 (Trimble, 2015). Lastly, the output image generated by the segmentation (Fig.8) was used and applied for the extraction of the ocher classes.
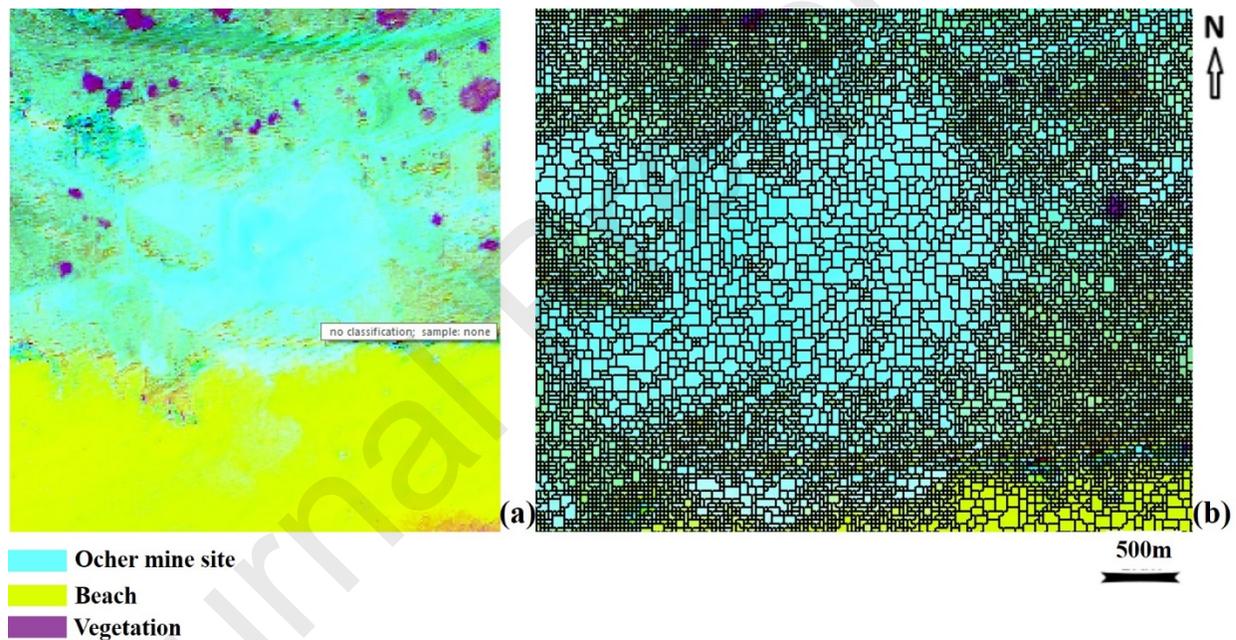

■ Ocher mine site
■ Beach
■ Vegetation

Fig. 8. a) The location of ocher mine without segmentation in RGB 473 of WV-3 data, and b) the location of ocher mine segmented by bottom-up strategy.

4.4. Training area and feature selection

In order to discern features of ocher listed in Table 2 and to define them based on the index bands the spectral characteristics of the ocher associated with individual mines was used. The OBIA method can measure various parameters; thus, several object features were extracted.

The image objects and their embeddings in the image object hierarchy were evaluated in index bands for calculating the object features. The ocher features and local variables were considered in scene, hierarchy, shape, and thematic layers. Furthermore, the position of ocher object in available scene was identified, and values of texture features based

on thematic layers and shape were extracted. Information about feature variables of ocher within the image and lithological object hierarchy were obtained to evaluate features of ocher deposits.

Additional object feature information including mean, standard deviation, minimum and maximum pixel values, hue, saturation, and intensity were extracted from index bands while features containing brightness, density, compactness, and homogeneity were assigned as the main factors for selecting training areas based on the index bands (Table 3). Indeed, the higher spectral and spatial resolutions of WV-3 extend the knowledge of features and provide detailed and precise information that can be used for complex mapping of ocher patterns not achievable by current multispectral imagery. The ocher mines 1, 2, and 3 were used for extracting training areas. The number of selected objects for training areas in each mine was 5, 10, and 8, respectively. These various object features were helpful for analysis of numerical differences and similarities of index bands for selection of ocher training areas.

Table.3. Features of WV-3 imagery used for selecting training areas of ocher

Ocher site/features	Number of objects	Features			
		Spectral measure	Shape measure		Texture measure
		Brightness	**Density**	**Compactness**	**Homogeneity**
Ocher Site1	1	201.66	1.704	1.235	1.00
	2	204.15	1.641	1.146	0.884
	3	207.72	1.693	1.200	1.00
	4	206.40	1.867	1.316	0.913
	5	208.94	1.865	1.155	0.873
Ocher Site2	1	204.19	1.718	1.385	1.00
	2	205.49	1.788	1.167	0.860
	3	201.31	1.642	1.167	0.873
	4	202.65	1.563	1.324	1.00
	5	202.68	1.535	1.154	1.00
	6	204.01	1.812	1.194	0.917
	7	201.15	1.851	1.207	1.00
	8	207.36	1.594	1.167	0.894
	9	206.37	1.648	1.355	1.00
	10	206.95	1.621	1.191	0.912
Ocher Site3	1	208.54	1.570	1.000	0.727
	2	208.49	1.805	1.321	1.000
	3	208.13	1.684	1.210	0.958
	4	206.44	1.862	1.146	0.769
	5	203.06	1.675	1.302	1.000

13

	6	202.64	1.851	1.241	0.904
	7	207.27	1.637	1.210	1.000
	8	202.58	1.793	1.185	0.915

4.5. Extraction of ocher potential **areas**

For easier identification of ocher in image objects, the lithological classes were added to ocher class. Considering the fixed numerical range of known ocher mines as a reference, the fixed numerical range of general and specific features of ocher in index bands of WV-3 including values of mode, mean, standard deviation, minimum and maximum pixel values, hue, saturation, and intensity were achieved. The numerical range of pixels in bands 2, 3, and 7 were 815-975 nm, 930-1052 nm, and 1721-1904 nm, respectively.

These ranges were selected for creating threshold conditions when applying "assign class" algorithm. The threshold condition for identification of ocher-rich areas is: "choose numbers between 815 and 975 for band 2, between 930 and 1052 for band 3, and > than 1700 for band 7" in object feature standard deviations, and "choose numbers between 1000 and 1100 for band 2, 1300 and 1600 for band 3, and 1800 and 2000 for band 7" in object feature saturation.

In this phase, thresholds for other classes are not calculated, and to create non-ocher layer, the class filter parameter was applied. The ocher-rich areas were delineated by a blue outline, while ocher mines were delineated by a yellow outline using gray image background (Fig. 9). Comparison of ocher-rich areas with previously mapped lithologies of Hormuz Island (Shayeganpour et al. 2021) and field controls indicated that the enhanced areas of ocher are compatible with the "mixed red soil, gypsum and anhydrite" rock unit which dominantly consists of iron oxides.

The results obtained by XRF analysis of ocher samples collected from known mines and samples collected from OBIA output areas are shown in Table 4. The XRD analysis showed major and minor phases of hematite, goethite, illite, gypsum, quartz, anhydrite, and calcite, in range of > 0 to 1.

Table.4. Results of XRF analysis of ocher samples (abundances in percent).

Sampling area	Sample name	Fe_2O_3	Al_2O_3	SiO_2	Na	CaO	SO_3
	Site1	10.04	2.86	9.95	1.24	21.40	10.32
Mine	Site 2	25.45	1.50	24.34	4.61	11.12	17.70
	Site 3	14.85	5.19	37.02	2.97	24.31	35.12
	Object1	14.85	1.50	9.95	2.97	11.12	17.70
OBIA	Object2	25.45	2.38	21.53	3.91	14.36	23.44

14

| result | Object3 | 12.25 | 2.86 | 24.34 | 4.61 | 24.31 | 35.12 |

The high-resolution spectral curves and the resampled spectra to WV-3 VNIR's spectral bands for a total of 3 locations, a mine site, and two ocher potential areas are shown in Figure 10; results from the XRF and XRD analysis are also revealed for easier comparisons. These showed that object-based image analysis method is a practical and efficient approach for enhancing ocher-rich areas. This mineral exploration method identifies specific and potential rock units as objects and investigates their absorption and reflection features compared to spectral bands. In image processing stage, the known mine sites were used as training areas for identifying similar districts. OBIA method applies the spectral features of target materials in imagery and uses objects' shape, texture, and geometry.

Taking into account that ocher is a mixture of iron oxide/hydroxide, and clay minerals, it could not be defined only based on the spectral features of one component; thus, we used the training areas collected from known ocher mines. At the same time, the accuracy of enhanced ocher-rich areas depends on the presence of mine site objects and their dependent factors. Mixture of any other material in ocher, even in low concentrations, can reduce the accuracy of the results. WV-3 VNIR data have a 1.24-meter spatial resolution which is considerably higher than multispectral imagery such as ASTER which is characterized by pixel sizes of 15 and 30 meters in VNIR-SWIR regions; thus, the output of applied method on WV-3 can show higher accuracy as a result of high homogeneity and purity achieved by object enhancements. Based on the calculated values for accuracy assessment (Table 5), the overall accuracy and Kappa coefficient for enhanced deposits of ocher are 88 % and 0.82. The user's and producer's accuracies were also calculated and shown in the same table. The most reliable controlling sites for accuracy assessment were the known ocher mines, which are revealed in Figure 9.
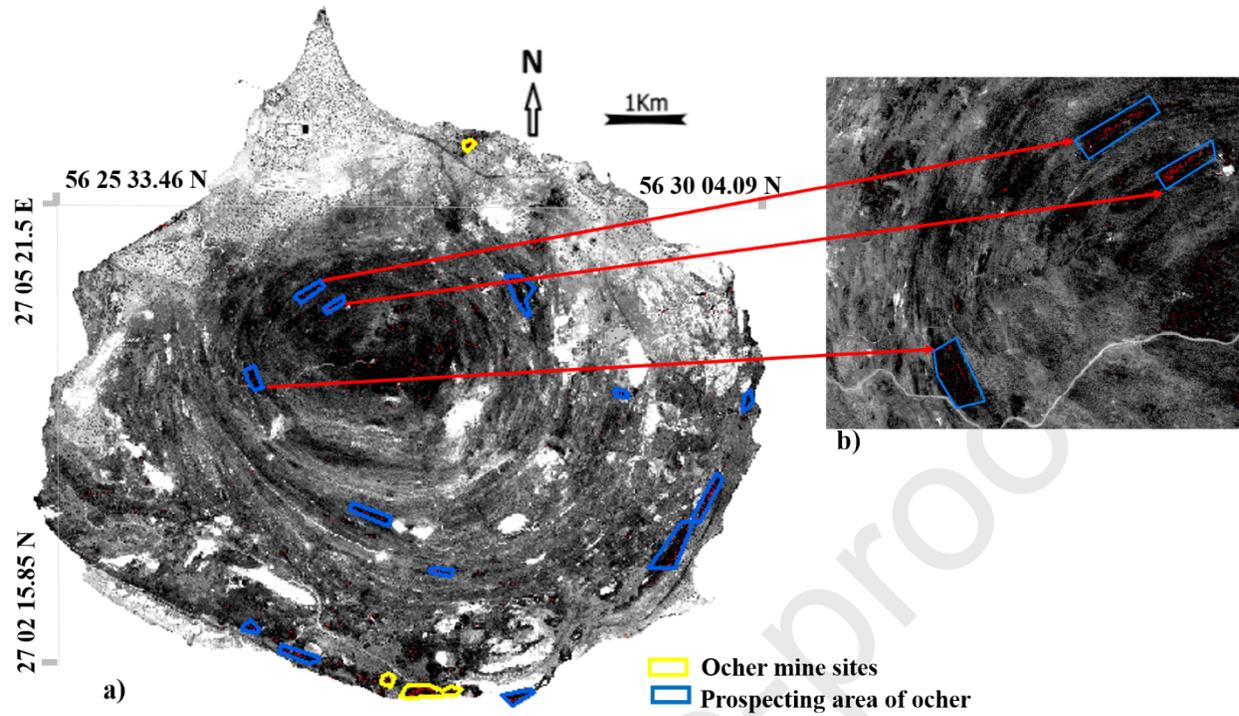
Fig. 9. a) ocher-rich areas in Hormuz Island indicated by OBIA method (blue boxes) and the active ocher mines (yellow boxes), b) close view of ocher-rich areas.

Table.5. Confusion matrix for results obtained by OBIA method

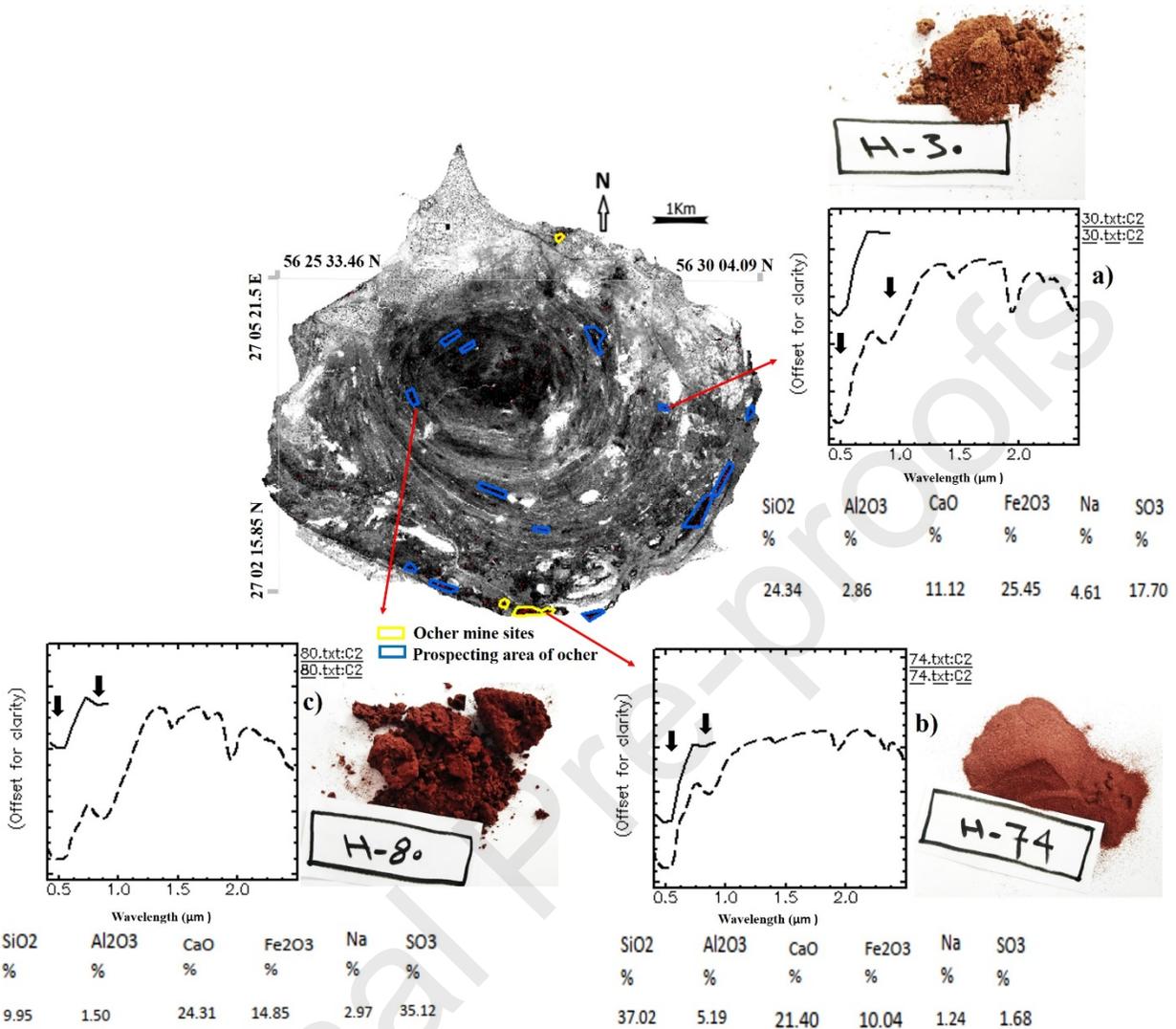|	Ocher (object)	Non-ocher (object)	Total (object)	User's accuracy
Ocher	85623	18984	104607	81.85
Non-ocher	10241	65487	75728	86.47
Total	95864	84435	180299	
Producer's accuracy (%)	89.31	77.55		

Fig. 10. Comparison of three ocher potential areas for spectral features, hand sample specifications, XRF, and XRD analysis; "a" and "c" are the ocher-rich areas prospected by this work, and "b" is the known ocher mine.

5. Conclusions

The efficacy of WV-3 VNIR data for exploring ocher deposits in Hormuz Island, southern Iran, was examined by applying OBIA and "assign class" algorithm using suitable threshold conditions. Using high-resolution spectral analyses, we found that spectral features of the ocher are typically similar to the spectra of a mixture of iron oxide/hydroxide and clay minerals.

Bands 3 and 4 were selected as absorption feature indicators, and bands 5 and 6 were selected as reflectance feature indicators. A multi-resolution segmentation algorithm was applied for iterative and sequential grouping of pixels. The ocher features and their local variables were analyzed based on the training and testing areas. Threshold condition and assign class algorithm were used to identify ocher-rich areas which provided potential locations for new ocher

prospects. Field observation, XRD and XRF analysis, and reflectance spectroscopy of samples collected from enhanced areas confirmed the occurrence of ocher in these areas. OBIA which is a relatively new and promising method was implemented for the enhancement of the ocher deposits in the salt dome areas. This research showed that integrating WV-3 data with OBIA approach reduces the need for extensive field observations, and the methodology is efficient for discriminating occurrences of relatively pure ocher in a lithologically complex system. This approach could also help prospect the minerals such as halite, potash, red soil, gypsum, oligist, and dolomite exposed in such areas, and other geologically similar systems.

6. References

Aqanabati, S.A. (2006). Geology and Mineral Potential of Hormozgan Province. *Journal of Development of Geology Training*, 12:4-11

Blaschke, T., Burnett, C., & Pekkarinen, A. (2004). New contextual approaches using image segmentation for object-based classification. In: De Meer F, de Jong S, eds. *Remote Sensing Image Analysis*: Including the spatial domain. Dordrecht: Kluver Academic Publishers, 211–236.

Bosak, P., Jaros, J., Spudil, J., Sulovsky, P., & Vaclavak, V. (1999). Salt plugs in the eastern Zagros, Iran: regional geological reconnaissance. *GeoLines* (Praha) 7, 3–174.

Burnett, C., & Blaschke, T. (2003). A multi-scale segmentation/object relationship modelling methodology for landscape analysis. *Ecological Modelling* 168, 233–249. https://doi.org/10.1016/S0304-3800(03)00139-X

Bedini, E. (2019). Application of WorldView-3 imagery and ASTER TIR data to map alteration minerals associated with the Rodalquilar gold deposits, southeast Spain. *Advances in Space Research*. https://doi.org/10.1016/j.asr.2019.01.047.

Bishop, J. L., Pieters, C. M., & Edwards, J. O. (1994). Infrared spectroscopic analyses on the nature of water in montmorillonite. *Clays and Clay Minerals, 6,* 702–716.

Congalton, R. (1991). A review of the assessing the accuracy of classification of remotely sensed data. *Remote Sensing of Environment*, *37*: 35–46.

Cloutis, E. A., Asher, P. M., & Mertzm, S. A. (2002). Spectral reflectance properties of zeolites and remote sensing implications. *Journal of Geophysical Research,* 107(E9), 5067. https://doi.org/10.1029/2000JE001467.

Clark, R. N., King, T. V. V., Klejwa, M., Swayze, G. A., & Vergo, N. (1990). High spectral resolution reflectance spectroscopy of minerals. *Journal of Geophysical Research,* 95, 12653– 12680.

Chen, Q.D., Deng, R.R., & Chen, L. (2014). Atmospheric correction of WorldView-2 data for the Xisha Island and reefs imagery. *Journal of Tropical Oceanography*, 33: 88-94

Clark, R. N., Swayze, G. A., Wise, R., Livo, E., Hoefen, T., Kokaly, R., & Sutley, S. J. (2007). USGS digital spectral librarysplib06a: U.S. *Geological Survey*, Digital Data Series 231. http://speclab.cr.usgs.gov/spectral.lib06.

Dwevedi, A., Kumar, P., Kumar, Y., Sharma, Y.K., & Kayastha, A.M. (2017). *Soil sensors: detailed insight into research updates, significance, and future prospects. New Pesticides and Soil Sensors*. Pages 561-594. doi.org/10.1016/B978-0-12-804299-1.00016-3

Elyasi, J., Aminsobhani, E., Behzad, A., Moeinvaziri, H. & Meysami, A. (1975). Geology of Hormoz Island. Geological Survey of Iran Publication, Tehran, 1, 13.

Eslami, A., Ghaderi, M., Rajendran, S., Pour, A. B., & Hashim, M. (2015). Integration of ASTER and landsat TM remote sensing data for chromite prospecting and lithological mapping in Neyriz ophiolite zone, south Iran. *Resource Geology*, 65(4): 375-388. https://doi.org/10.1111/rge.12076

Escribano, E., Schmid T., Chabrillat S., Rodríguez-Caballero E., & García, M. (2017). *Optical Remote Sensing for Soil Mapping and Monitoring*. Soil Mapping and Process Modeling for Sustainable Land Use Management. Pages 87-125. doi.org/10.1016/B978-0-12-805200-6.00004-9.

Faramarzi, N.S., Amini, S., Schmitt, A.K., Hassanzadeh, J., Borg, G., McKeegan, K., Razavi, S.M.H., & Mortazavi, S.M. (2015). Geochronology and geochemistry of rhyolites from Hormuz Island, southern Iran: A new record of Cadomian arc magmatism in the Hormuz Formation. *Lithos,* 236–237, 203–211. https://doi.org/10.1016/j.lithos.2015.08.017

Forouzan, M., & Arfania, R. (2020). Integration of the bands of ASTER, OLI, MSI remote sensing sensors for detection of hydrothermal alterations in southwestern area of the Ardestan, Isfahan Province, Central Iran. *The Egyptian Journal of Remote Sensing and Space Sciences,* 23: 145–157

Ghorbani, M. (2013). *The Economic Geology of Iran, Mineral Deposits and Natural Resources*. ISBN: 978-94-007-5625-0. Pages 65-78.

Grebby, S., Field, E., & Tansey, K. (2016). Evaluating the Use of an ObjectBased Approach to Lithological Mapping in Vegetated Terrain. *Remote Sensing*, 8(10): 843.

Gaffney, E. S., Singer, R. B., & Kunkie, T. D. (1984). *Zeolites on mars: Prospects for remote sensing, in reports of the planetary geology and geophysics program 1984* (p. 397). Washington, D. C.: NASA.

Hunt, G. R. (1977). Spectral signatures of particulate minerals in the visible and near infrared. *Geophysics,* 42(3): 501–513.

Hewson, R.D., Chinkaka, E., van der Meijde, M., Baugh, B., Titus, N., & Mubita, J.P. (2019). Geological investigations with high spatial resolution WV-3 satellite imagery and regional geophysics at the Haib Cu porphyry, Namibia. ASEG Extended Abstracts 2019, 1–5. https://doi.org/10.1080/22020586.2019.12073089

Karale, R.L., Bali, Y.P., & Seshagiri Rao, K.V. (1983). Soil mapping using remote sensing techniques. *Indian Acad*, *Sci*. (Engg. Sci.), 6. 3: 197-208.

Karimzadeh, S., H. & Tangestani, M. (2021). Evaluating the VNIR-SWIR datasets of WorldView-3 for lithological mapping of a metamorphic-igneous terrain using support vector machine algorithm; a case study of Central Iran. *Advances in Space Research*, 68, 2421–2440. https://doi.org/10.1016/j.asr.2021.05.002

Kauth, R.J. & Thomas, G.S. (1976). The Tasselled Cap—A Graphic Description of the Spectral-Temporal Development of Agricultural Crops as Seen by Landsat. LARS Symposia Paper 159. http://docs.lib.purdue.edu/lars_symp/159/

Radoux, J., & Bogaert, P. (2017). Good Practices for Object-Based Accuracy Assessment. Remote Sensing, 9(7). doi:10.3390/rs9070646

Lang, S., Schöpfer, E., & Langanke, T. (2008). Combined object-based classification and manual interpretation — Synergies for a quantitative assessment of parcels and biotopes. *Geocarto Internationa*, L 23 (4): 1–16.

Mars, J.C. (2018). Mineral and Lithologic Mapping Capability of WorldView 3 Data at Mountain Pass, California, Using True- and False-Color Composite Images, Band Ratios, and Logical Operator Algorithms. *Economic Geology,* 113, 1587–1601. https://doi.org/10.5382/econgeo.2018.4604

Nabavi & Agha Nabati, *Geological Survey of Iran.* 2001

Pour, A.B., & Hashim, M. (2012). Identifying areas of high economic-potential copper mineralization using ASTER data in the Urumieh-Dokhtar Volcanic Belt, Iran. *Adv. Space Res,* 49: 753–769.

Sun, Y., Tian, S., & Di, B. (2017). Extracting mineral alteration information using WorldView-3 data. *Geoscience Frontiers,* 8, 1051–1062. https://doi.org/10.1016/j.gsf.2016.10.008

Serbouti, I., Raji, M., Hakdaoui, M., Pradhan, B., Lee, C.-W., & Alamri, A.M. (2021). Pixel and Object-Based Machine Learning Classification Schemes for Lithological Mapping Enhancement of Semi-Arid Regions Using Sentinel-2A Imagery: A Case Study of the Southern Moroccan Meseta. *IEEE Access,* 9, 119262–119278. https://doi.org/10.1109/ACCESS.2021.3107294

Stocklin, J. (1972). Lexique Stratigraphique International. Vol. 3, Geological Survey of Iran Publication, Tehran, 6, 15.

Shayeganpour, S., Tangestani, M.H., Gorsevski, P.V. (2021a). Machine learning and multi-sensor data fusion for mapping lithology: A case study of Kowli-kosh area, SW Iran. *Advances in Space Research*, 68, 3992–4015. https://doi.org/10.1016/j.asr.2021.08.003

Shayeganpour, S. Tangestani, M.H., Homayouni, S., & Vincent, R.K. (2021b). Evaluating pixel-based vs. object-based image analysis approaches for lithological discrimination using VNIR data of WorldView-3. *Front. Earth Sci*, 20848-TMH.3d 3/2/021 15:27:52. doi.org/10.1007/s11707-020-0848-7.

Salehi, T., & Tangestani, M.H. (2019). Large-scale mapping of iron oxide and hydroxide minerals of Zefreh porphyry copper deposit, using Worldview-3 VNIR data in the Northeastern Isfahan, Iran. *Int J Appl Earth Obs Geoinformation*, 73: 156–169.

Singh, S. (2016). Remote sensing applications in soil survey and mapping: A Review. *International Journal of Geomatics and Geosciences*, 7(2): 192-203.

Sun, Y., Tian, S., & Di, B. (2017). Extracting mineral alteration information using WorldView-3 data. Geosci. *Front*, 8: 1051–1062

Thomas, A., Rider, M., Curtis, A., & MacArthur, A. (2011). Automated lithology extraction from core photographs. First Break 29. https://doi.org/10.3997/1365-2397.29.6.51281

Trimble, (2015). eCognition Developer 9.1 User Guide*;* Trimble Documentation: Munich, Germany

Kuester, M., (2016). *Radiometric use of WV-3 imagery*. Technical Note. DigitalGlobe p. 12. WorldView3.digitalglobe.com.

Kruse, F., & Perry, S. (2013). Mineral Mapping Using Simulated Worldview-3 Short-Wave-Infrared Imagery. *Remote Sensing,* 5, 2688–2703. https://doi.org/10.3390/rs5062688

Tormos, T., Kosuth, P., Durrieu, S., Dupuy, S., Villeneuve, B., & Wasson, J. (2012). Object-based image analysis for operational fine-scale regional mapping of land cover within river corridors from multispectral imagery and thematic data. *International Journal of Remote Sensing*, 33: 4603–4633. DOI: 10.1080/01431161.2011.637093.

Ye, B., Tian, S., Ge, J., & Sun, Y. (2017). Assessment of WorldView-3 Data for Lithological Mapping. *Remote Sensing,* 9, 1132. https://doi.org/10.3390/rs9111132

Yu. H.Y., Li, F.B., Liu, C.S., Huang, W., Liu, T.X., & Yu, W.M. (2016). Iron Redox Cycling Coupled to Transformation and Immobilization of Heavy Metals: Implications for Paddy Rice Safety in the Red Soil of South China. *Advances in Agronomy*, 137: 279-317. doi.org/10.1016/bs.agron.2015.12.006

Whiteside, T. G., Maier, S. W., & Boggs, G. S. (2014). Area-based and location-based validation of classified image objects. International Journal of Applied Earth Observation and Geoinformation, 28, 117-130. doi:https://doi.org/10.1016/j.jag.2013.11.009

Yazdi, A., Emami, M.H. & Jafari, H.R. (2013). IRAN, the Center of Geotourism Potentials. *Journal of Basic and Applied Scientific Research*, *3*: 458-465.

Yang, Y., Zhang, Z., Tang, J.X., Chen, Y.C., Li, Y.B., Wang, L.Q., Li, J.L., Gao, K., Wang, Q., & Yang, H.H. (2015). Mineralization, alteration and vein systems of the Bolong porphyry copper deposit in the Duolong ore concentration area, Tibet. *Geol. China, 42*: 759–776.

Zhang, G.K., Chen, C, & Xing, F. (2008). Spectral radiometric calibration research of Quick Bird digital image Spectroscopy and Spectral Analysis, 28: 494-498.

Zhan, Q., Molenaar, M., Tempfli, K., & Shi, W. (2005). Quality assessment for geo-spatial objects derived from remotely sensed data. International Journal of Remote Sensing, 26(14), 2953-2974. doi:10.1080/01431160500057764